1951–2021
LINCOLN LABORATORY
MASSACHUSETTS INSTITUTE OF TECHNOLOGY
244 Wood Street, Lexington, Massachusetts 02421

Improved Hyperspectral IR/Microwave Sounding of Boundary Layer Inversions: FINAL REPORT

2 February 2024

SUBMITTED BY:

Dr. Adam B. Milstein
Applied Space Systems Group, MIT Lincoln Laboratory
Phone: 781-981-6870
E-mail: milstein@ll.mit.edu

This material is based upon work supported by the National Aeronautics and Space Administration under Air Force Contract No. FA8702-15-D-0001. Any opinions, findings, conclusions or recommendations expressed in this material are those of the author(s) and do not necessarily reflect the views of the National Aeronautics and Space Administration.

Contents

1. INTRODUCTION

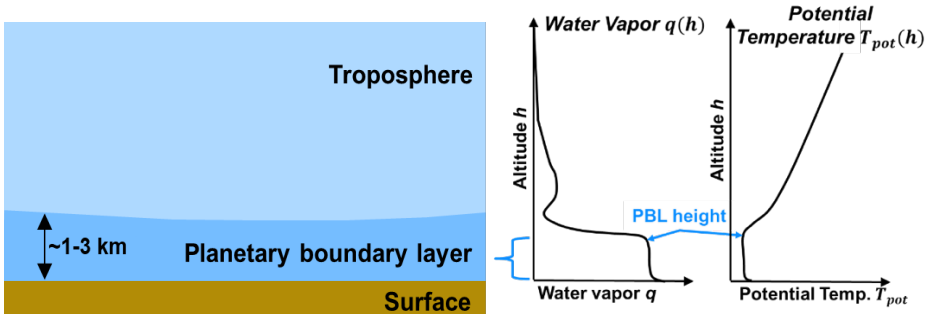

Figure 1: Planetary boundary layer (PBL) illustration, and illustrated water vapor and potential temperature profiles showing sharp gradient at the top of the PBL (from [1])

(Note: Contents of this chapter first appeared in [2].)

Improved understanding of thermodynamics within the Planetary Boundary Layer (PBL), including its structure and PBL height (PBLH) over land and water as a function of time of day, is of great importance to NASA, as recommended by the National Academy of Sciences in the 2017 Decadal Survey for Earth Science and Applications from Space ("ESAS 2017") [3, 4] and subsequently by the NASA PBL Incubation Study Team Report (STR; [5]). During the ESAS 2017 process, improved PBL monitoring from space was identified as a high priority across multiple interdisciplinary panels and science and application questions, leading to the current NASA PBL Decadal Survey Incubation (DSI) program that will invest in future spaceborne PBL mission development. [2]

In recent decades, spaceborne microwave and hyperspectral infrared (HIR) sounding instruments on Aqua, Suomi NPP, and JPSS have significantly improved weather forecasting [6, 7]. However, existing retrievals of lower troposphere temperature T and water vapor q profiles from HIR and microwave sounders have limitations in vertical resolution, and often cannot accurately represent key features such as the mixed layer thermodynamic structure and the inversion at the PBL top, the latter of which appears as a sharp gradient in q or potential temperature T_{pot} as illustrated in Figure 1. With the mixed layer itself being ~1-3 km thick, previously reported AIRS T and q profile resolution (and resultant PBLH) errors on the order of ~1-2 km [8] are not sufficient, and, alone, fall well short of the ESAS recommendation of ~100-300 m vertical resolution for new PBL observing systems. **Because of the existing limitations in PBL remote sensing from space, there is an urgent need to improve routine, global observations of the PBL and enable advances in scientific understanding and weather and climate prediction.** In addition, existing program of record (POR) satellite measurements such as those from HIR have not been the focus of targeted PBL retrieval assessment or development to date, which is particularly critical as NASA considers what next-generation sensors or observing systems will needed to address PBL needs. With the HIR sensor record continuing beyond the next decade with SNPP, JPSS, IASI, and planned GEO sounders, new methodologies that improve sounding capability will yield benefit for a long time to come. We therefore summarize the key questions we investigate as follows:

- What is the upper limit of HIR vertical sounding capability in the PBL?
- How can both AI and physics be used to constrain retrieval estimates in an explainable way, and improve upon current state-of-the-art retrieval approaches? [2]

In this report, we describe how some of our recent efforts have made progress toward addressing these questions. This document updates a previous report [2] addressing similar subject matter with additional, more recent work funded by the Science of Terra and Aqua 2017 element.

2. CURRENT RETRIEVAL APPROACHES

(Note: Contents of this chapter first appeared in [2].)

Sounding retrieval algorithms reconstruct a vertical distribution of atmospheric temperature and water vapor from the observations, which consist of thermal IR and microwave radiation emitted by layers of the atmosphere and measured by a sounder instrument on orbit [9]. The objective is to estimate the state of the atmosphere (represented by unknown parameter vector x, a vertical profile of $T(p)$ or $q(p)$, given spaceborne spectral radiance observations (represented by a radiance vector y). The IR observations used in y are typically a cloud-cleared spectrum derived from a 3 by 3 group of neighboring cloudy spectra beforehand (though single-FOV retrievals have recently advanced [10] as well). This inverse problem is ill-posed, lacking a single unique solution, with vertical details beyond a certain (scene- and data-dependent) vertical resolution limit not directly observable from the spectral measurements, including in the lower troposphere and the PBL. As highlighted below, this limitation in PBL information content from the instrument motivates the need for the new, AI-informed techniques described herein. [2]

Two approaches to sounding retrievals are described in Figure 2: physical retrievals and statistical regression retrievals. The physical retrieval approach uses a forward model (the radiative transfer model) to calculate the expected measurements $f(x)$ given a specific atmospheric state x. The estimate $\hat{x}$ is iteratively adjusted to reduce the squared difference between the observations y and prediction $f(\hat{x})$. Due to ill-posedness, an additional regularization term is required to stabilize the retrieval, often taking a form similar to what is shown in Figure 2, in which a penalty for deviations from a first guess x_{prior} is imposed. Statistical regression approaches, including neural networks, learn an empirical relationship $\hat{x} = z(y)$ between an ensemble of measurements $y_{ensemble}$ and collocated ground truth datasets $x_{ensemble}$ [11]. For a neural network, $z(\cdot)$ is a nonlinear function composed of simple, interconnected computational elements, or nodes, defined by learned weight parameters and an activation function. A key advantage for neural networks over physical approaches is that they are fast and accurate, and, as universal function approximators [12], they can empirically learn complex, often indirect and nonlinear dependencies embedded in the data that may be difficult to physically model[11]. A key advantage of physical retrievals over statistical retrievals is that they are directly explainable, meaning that it is clear what part of the solution is introduced from the instrument radiances versus propagated from the first guess. Neural networks have attracted increasing wide from the sounding community in recent years [2, 13-16]

In recent years, the Level 2 retrieval algorithm for Aqua's Advanced Microwave Sounding Unit (AMSU) has combined both of these approaches by using MIT-LL's Stochastic Cloud Clearing/Neural Network (SCC/NN) retrieval [17, 18] as first guess for NASA GSFC's physical retrieval. The introduction of SCC/NN as the first guess has led to improved accuracy and yield in down to the surface, including the PBL, versus previous versions with a different regression first guess[19]. In the current retrievals, PBL phenomenology is, to a significant degree, introduced via the SCC/NN first guess. This combination of neural networks and physical retrieval to improve operational science products resulted from over a decade of investment by NASA, long predating the recent intensified focus on AI from the larger science and technology community. [2]

Physical Retrieval	
$\hat{\boldsymbol{x}} = \text{argmin}_{\boldsymbol{x}}\left\{\|\boldsymbol{y}-\boldsymbol{f}(\boldsymbol{x})\|_{\boldsymbol{\Lambda}}^2 + \|\boldsymbol{x}-\boldsymbol{x}_{\text{prior}}\|_{\boldsymbol{B}}^2\right\}$	
$\boldsymbol{x}$	Unknown *T(p)* or *q(p)* profile
$\boldsymbol{y}$	Spectrum measurements
$\boldsymbol{f}(\cdot)$	Forward model
$\boldsymbol{\Lambda}, \boldsymbol{B}$	Meas. and prior inverse covariances
$\boldsymbol{x}_{\text{prior}}$	First guess of *T(p)* or *q(p)*

Neural Network Retrieval
$\hat{\boldsymbol{x}} = \boldsymbol{z}(\boldsymbol{y})$, where $\boldsymbol{z}(\cdot)$ is a neural network, trained using:
$\text{argmin}_{\boldsymbol{z}(\cdot)}\{\|\boldsymbol{x}_{\text{ensemble}} - \boldsymbol{z}(\boldsymbol{y}_{\text{ensemble}})\|^2\}$

Figure 2: Physical versus neural network retrieval approaches for atmospheric sounding **[2]**

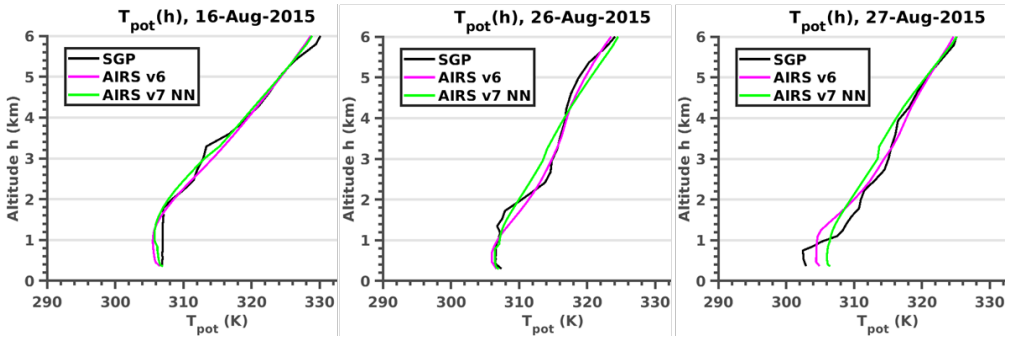

Figure 3: PBL T_{pot} profiles for ARM-SGP, AIRSv6, AIRSv7 NN (From **[2]**)

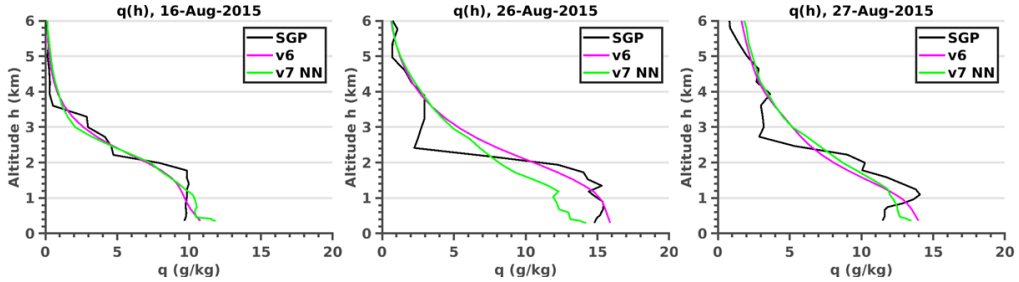

Figure 4: PBL q profiles for ARM-SGP, AIRSv6, AIRSv7 NN (From **[2]**)

Despite these recent improvements, further efforts are needed to both understand and improve performance in the PBL. Figure 3 shows three example afternoon T_{pot} retrievals from AIRS/AMSU compared collocated radiosonde truth profiles at the Southern Great Plains (SGP) site in Oklahoma operated by the Atmospheric Radiation Measurement (ARM) facility in 2015[20]. The AIRS/AMSU retrievals include the version 6 ("AIRS v6") product, and the NN first guess for the new v7 product ("AIRS v7 NN") which aimed for PBL improvements. Figure 4 shows an analogous set of plots for q profiles. The collocations used the nearest profiles flagged as high quality down to the surface, and are therefore best-case matchups. Nevertheless, the examples illustrate limitations in current capability addressed by this proposal. Profiles tend to be overly smooth, with relatively weak vertical gradients compared to the sonde profiles due to limited information in the lower troposphere. As a result, distinguishing between the well-mixed layer and the PBL top inversion is difficult, as is accurate determination of PBLH. This problem is especially apparent for q, where we have noted significant room for improvement. [2]

3. MAP ESTIMATION AND VARIABLE SPLITTING FRAMEWORK

(Note: Contents of this chapter first appeared in [2].)

A traditional approach to solving the physical retrieval problem is known as optimal estimation"[9], or maximum a posteriori (MAP) estimation. Here, we review MAP estimation, and then we use it to motivate a more general framework. We define, again, observations y and unknown atmospheric state x (describing temperature T and humidity q). [2]

$$\begin{aligned}\hat{x} &= \arg\max_x \{\log p(y|x) + \log p(x)\} \\ &= \arg\max_x \{(\text{data fitting term}) + (\text{regularization term})\}\end{aligned} \quad \textbf{(1)}$$

The data likelihood $p(y|x)$ describes how well the observations y match predictions $f(x)$, and is typically assumed normally distributed with inverse measurement covariance as in Figure 2:

$$\log p(y|x) = -\frac{1}{2}\|y - f(x)\|_\Lambda^2 + (\text{const.}) \quad \textbf{(2)}$$

In principle, the prior model $p(x)$ describes how the set of all x should be distributed, including complicated joint dependencies. In practice, a model $p(x)$ is chosen to regularize the MAP solution with certain key properties expected of x, like proximity to a first guess or a resolution limit, that can be captured in a tractable cost function, and it is typically assumed Gaussian, as shown in the example in Figure 2. We define $g(x) = -\log p(y|x)$ and $h(x) = -\log p(x)$, so that

$$\hat{x} = \arg\min_x \{g(x) + h(x)\} \quad \textbf{(3)}$$

For many typical choices of $g(x)$ and $h(x)$, (3) can be solved using nonlinear least squares optimization techniques such as the Levenberg-Marquardt technique[9], or analogous techniques. Here, we use a different approach, known as "variable splitting", with the aim of enabling the use of a wider variety of options for $h(x)$, including non-Gaussian models [21-23]. Suppose we split x into two different variables, x_1 and x_2, and minimize $g(x_1) + h(x_2)$ such that $x_1 = x_2$ as follows:

$$\begin{aligned}(\hat{x}_1, \hat{x}_2) &= \arg\min_{x_1 = x_2} \{g(x_1) + h(x_2)\} \\ &= \arg\min_{x_1, x_2} \left\{ g(x_1) + h(x_2) + \frac{1}{2\sigma^2}\left|\left|x_1 - x_2 + u\right|\right|^2 \right\}\end{aligned} \quad \textbf{(4)}$$

where u is an "augmented Lagrangian" to be solved for, similar to a Lagrange multiplier, and σ is a selectable parameter which controls the rate of convergence. This problem can be solved with a series of update steps that alternate among all the unknowns. This scheme, called "Alternating Direction Method of Multipliers" (ADMM)[21, 22], is powerful because it enables solution of a difficult, constrained optimization problem as a sequence of simpler unconstrained steps:

- Initialize $u = 0$
- Repeat until converged:
  - $\hat{x}_1 = \arg\min_{x_1} \left\{ g(x_1) + \frac{1}{2\sigma^2}\left|\left|x_1 - \hat{x}_2 + u\right|\right|^2 \right\}$ *// Sensor model update step*
  - $\hat{x}_2 = \arg\min_{x_2} \left\{ h(x_2) + \frac{1}{2\sigma^2}\left|\left|\hat{x}_1 - x_2 + u\right|\right|^2 \right\}$ *// Prior model update step*
  - $u = u + (\hat{x}_1 - \hat{x}_2)$ *// "Augmented Lagrangian"*

We can define the following functions, which are called "proximal maps", corresponding to the above update steps as follows [2]:

$$G(x) = \arg\min_v \left\{ g(v) + \frac{1}{2\sigma^2} ||v - x||^2 \right\} \quad \textbf{(5)}$$
$$H(x) = \arg\min_v \left\{ h(v) + \frac{1}{2\sigma^2} ||v - x||^2 \right\}$$

Informally, we can interpret the proximal map as an "agent" that improves the current estimate:

- "Agent" that improves sensor model fit: $G(x) \approx x\text{-}\alpha\nabla g(x)$
- "Agent" that improves prior model fit: $H(x) \approx x\text{-}\alpha\nabla h(x)$

The above ADMM algorithm is then:

- Initialize $u = 0$
- Repeat until converged:
  - $\hat{x}_1 = G(\hat{x}_2 - u)$ *// Sensor model "agent"*
  - $\hat{x}_2 = H(\hat{x}_1 + u)$ *// Prior model "agent"*
  - $u = u + (\hat{x}_1 - \hat{x}_2)$ *// "Augmented Lagrangian"*

The ADMM alternates successive small improvements to the sensor model fit and prior model fits until convergence to a final result which strikes a balance between fitting both models. The prior model agent, in particular, tends to enhance the current estimate by denoising it or removing artifacts from it, bringing it closer into alignment with expected properties of valid solutions that the sensor model alone may not directly constrain. The convergence conditions are as follows:

$x = G(x - u)$ *// Sensor model agent*

$x = H(x + u)$ *// Prior model agent*

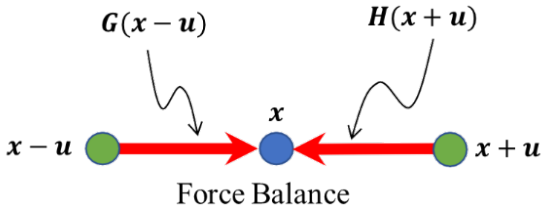

Figure 5: CE force balance illustration (From **[2]**)

These conditions have been introduced with the name "Consensus Equilibrium" (CE) by Buzzard et al.[23], evoking the idea of a "force balance" or "equilibrium" between multiple agents (in this case, the sensor model agent and the prior mode agent) acting on the estimate, as illustrated in Figure 5. [2]

4. RECENT TARGETED RETRIEVAL WORK AND APPLICATION TO PBL

(Note: Contents of this chapter first appeared in [2].)

Drawing on the previous sections, we can describe a sensor model agent as a proximal map, based on (2), with cloud cleared observations y and radiative transfer forward model $f(\cdot)$:

$$G(x) = \arg\min_{v}\left\{\frac{1}{2}\|y - f(v)\|_{\Lambda}^{2} + \frac{1}{2\sigma^{2}}||v - x||^{2}\right\} \quad \textbf{(6)}$$

An implementation of (6) for AIRS has already been developed on the existing 2017 TASNPP project, using the v7 SCC/NN retrieval as the clear state for cloud clearing and the Stand-alone Atmospheric Radiative Transfer Algorithm (SARTA) [24] forward model. Under this proposed work, we will draw on the team's experience on the existing AIRS and CrIS Level 2 retrieval algorithms [18, 25] to improve the current sensor agent for both sensors, improving error propagation, cloud clearing, and channel selection. For example, as part of the TASNPP effort AIRS/AMSU Level 2 retrieval performance was evaluated for a selection profiles collocated with a PBL-focused SGP radiosonde measurement campaign. The comparison showed that there is room for improvement in vertical resolution in the PBL via physical retrieval approaches, for q in particular, which subsequently became a subsequent area of focus. As a result, Milstein et al. developed a new approach for retrieving q, with the goal of making better use of the available radiances[26]. The approach starts with the v7 SCC/NN AIRS/AMSU retrieval as first guess accompanied by a newly developed per-retrieval uncertainty covariance estimate predicted using a Mixture Density neural network (described in [27]). This first guess is then used as a clear state and first guess for a new physical retrieval approach that differs in important ways from existing retrieval approaches: A total variation (TV) smoothness prior is used to regularize the solution while preserving sharp features. As Karl states in [28], "unlike standard quadratic Tikhonov solutions, total variation regularized answers can contain localized steep gradients, since the regularizer penalizes only the total amount of gradient in the image and not its distribution. As a result, edges are preserved in the reconstructions." In addition, the predicted first guess covariance estimate is employed as a bounds constraint (e.g., "stay within 1-sigma of the first guess"), rather than a Gaussian prior adding a quadratic norm penalty to the cost function. Other bounds constraints from physical realism such as avoiding oversaturation are also enforced. Combined, these priors avoid conventional Gaussian assumptions which tend to oversmooth regularized solutions and are therefore appropriate for PBL-focused q retrievals where a sharp gradient is expected. As illustrated in Figure 6, this approach can be described using the CE framework and alternating optimization approach of 3, with proximal map agents on a profile: a sensor agent similar to (6), a prior model agent that enforces bounds constraints relative to the first guess, and an additional prior agent that enforces the total variation prior model on the profile. [2]

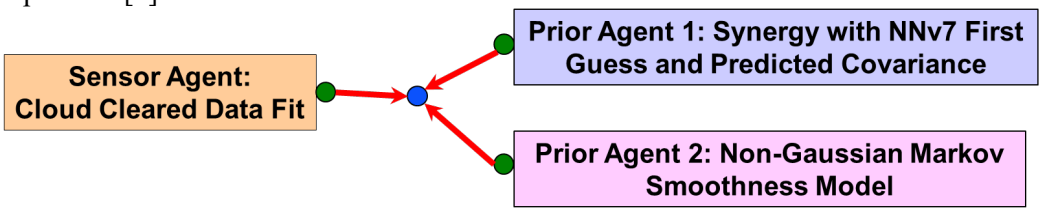

Figure 6: Illustration of the 2017 TASNPP analysis effort as a CE problem (From **[2]**)

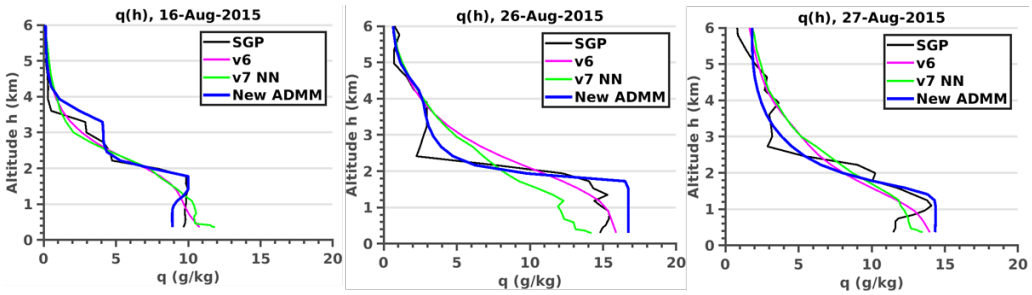

Figure 7: Example PBL *q* profiles for ARM-SGP, AIRSv6, AIRSv7 NN, and new ADMM approach. (From **[2])**

To evaluate this approach, these ADMM retrievals were added to those in Figure 4, and the results are shown in Figure 7. The ADMM profiles show more vertical structure, including inversions, near the PBL than the v6 and v7 SCC/NN retrievals. This work illustrates that significant improvement in resolving PBLH is possible using the proposed CE framework, incorporating more machine learning elements (such as first guess error prediction) and nontraditional, non-Gaussian prior models that preserve sharp gradient features of most interest in PBL retrievals. [2]

5. 3D SPATIAL ENHANCEMENT USING DEEP LEARNING

Despite recent improvements including fine structure contributed by SCC/NN in the AIRS/AMSU retrieval methodology and targeted investigations described in the previous chapters, retrievals from hyperspectral IR and microwave sounding instruments overall continue to have limited vertical resolution in the PBL. We investigated another approach for addressing these limitations: Treating the 3D T/q granule retrieved by SCC/NN as a 3D volumetric image, and applying 3D deep learning techniques to enhance detail and reduce noise by exploiting 3D spatial information. In a recent paper[1], we outlined our approach. We have called it Temperature and Humidity ATmospheric Sounding DEtail-Enhancing Prior (THATS-DEEP) and applied it to 3D granules (~1650 km wide) of T and q retrieved using the Version 7 SCC/NN retrieval (the AIRS product first guess) as the starting point.

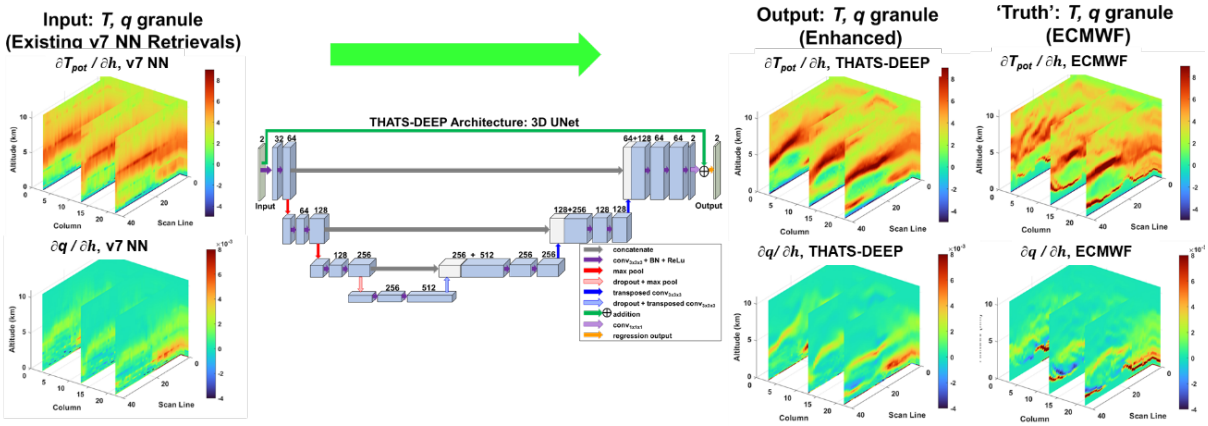

Figure 8: THATS-DEEP architecture and real example 3D granule images, the vertical gradients of potential temperature and moisture [1]

The deep neural network (DNN) we have developed is shown in Figure 8, and is based on the 3D UNet [29] architecture, with a mixed gradient [30] loss function. At execution, the inputs are the V7 SCC/NN retrieval granule, presented as a 3D image with a "temperature" channel and a "moisture" channel. (Here, "channel" is used analogously to how RGB are treated as 3 spatially coincident image "channels" in image processing applications.) The targets for training are T and q fields from ERA5, collocated spatially and temporally with the AIRS granule. Importantly, for training, the inputs we use are synthetic, but realistic, data similar to SCC/NN retrievals rather than actual retrievals. These synthetic inputs are derived from the ERA5 targets by applying simulated smoothing error and noise. State-dependent smoothing error is performed using a dedicated neural network trained for that purpose. This approach preserves exact spatial and temporal correspondence between the input and output when training that would not be available if the real SCC/NN retrievals had been used as training inputs. Training THATS-DEEP therefore does not require that the ERA5 fields are ground truth paired with the real retrievals – only that their 3D T/q phenomenology are physically realistic examples of the atmosphere, particularly in the PBL.

Example results are shown in Figure 9. The granule is for a July 16, 2010 UTC 11:53 daytime scene over Africa, and potential temperature T_{pot}, log(q), q, and vertical gradients of T_{pot} and q are plotted. The original SCC/NN granule, on the left, shows gradients which are characteristic of the top of a convective PBL, but they noisy and not clearly resolved. Following THATS-DEEP enhancement, the mixed layer is resolved more clearly, with visual quality more comparable to that of the collocated ERA5 (also shown), and vertical gradients far more apparent.

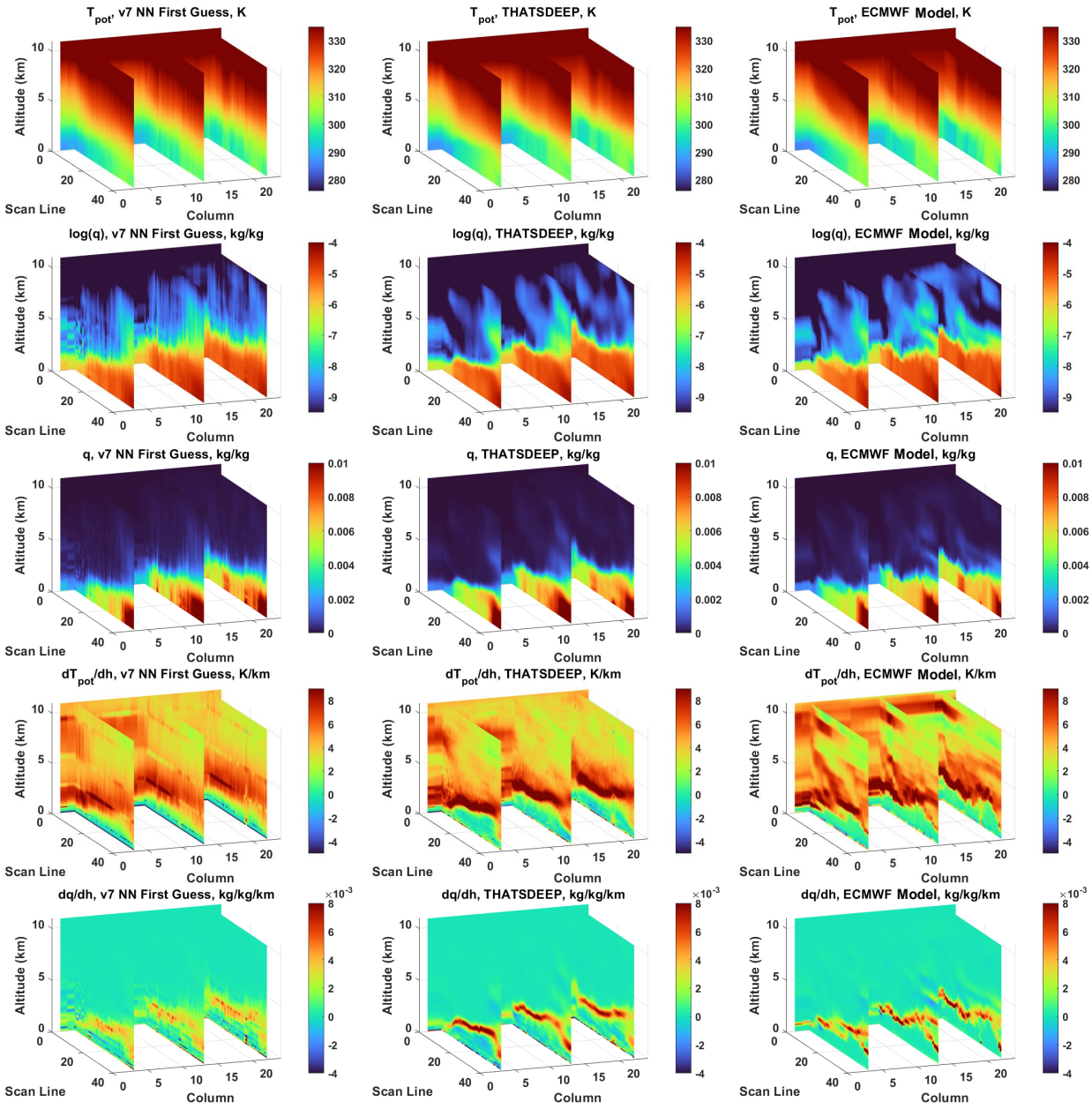

Figure 9: THATS-DEEP enhances detail of AIRS/AMSU v7 SCC/NN granule, with results looking more like ERA-5 reference in quality [1]

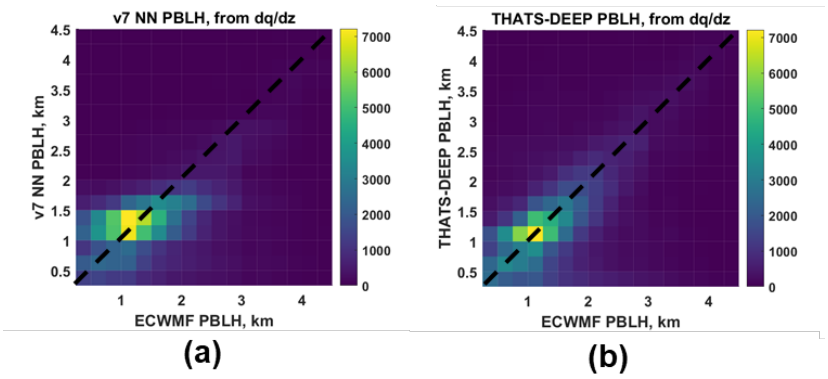

Figure 10: 2D histogram for PBLH for (a) v7 NN vs corresponding ECMWF profiles, (b) THATS-DEEP (with real v7 NN inputs), vs corresponding ECMWF profiles. PBLH was computed from the gradient of q [1]

To quantify performance over land, we assessed PBL height (PBLH) accuracy for both the v7 SCC/NN retrievals (which contribute fine structure in the PBL to the final retrievals) along with THATS-DEEP enhancement versus ERA5 for an ensemble of 149,622 profiles (daytime, |lat|<65, 2010 and 2013, land). To compute PBLH we used a vertical gradient approach similar to Seidel et al.[31]for q (and, in the paper [1] T_{pot}) individually. We use ERA5 here as a useful referee or "truth" comparison source, despite the fact that it is not an in situ measurement, as ERA5 has been shown to produce realistic estimates of PBL structure compared to observations [32], typically underestimating PBLH by ~130 m. Performance of retrievals versus ERA5 will therefore provide an upper bound to the actual errors due to the possibility of small errors in the ERA5 model.

Figure 10 plots a 2D histogram of PBLH computed from retrieved q, versus that of the corresponding ERA5 q profile. Figure 10(a) shows results for v7 SCC/NN, while Figure 10 (b) shows the results for THATS-DEEP with real v7 NN inputs. The central peak for THATS-DEEP-derived PBLH maintains a slope of approximately 1 with respect to the ERA5-derived PBLH with agreement within ~0.5 km (as seen in the peak's half-width). In contrast, the PBLH for v7 SCC/NN is less accurate, tending to remain concentrated between 1 and 2 km. To further quantify this, Figure 11 shows the median error (bias) and mean absolute error (MAE) of PBLH from retrievals versus from ERA5 as a function of altitude. The median error in Figure 11 (a) shows that bias in PBLH is reduced by THATS-DEEP at almost all altitudes

by roughly a factor of 2, while MAE in Figure 11 (b) shows reduction in MAE from THATS-DEEP for altitudes above 1.7 km.

A more in-depth presentation of these results and the analysis methodology are found in our paper [1].

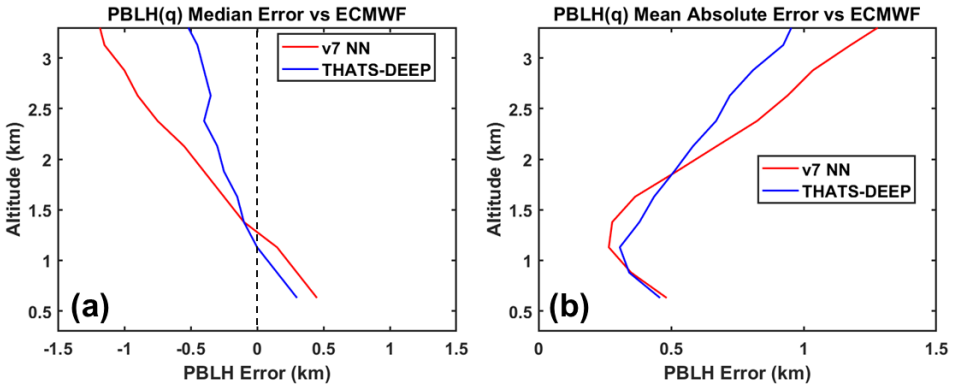

Figure 11: Quantitative PBLH results (from the gradient of *q*), including (a) median PBLH error versus ECMWF and (b) mean absolute error of PBLH versus ECWMF, for both v7NN and THATS-DEEP, as a function of altitude [1]

6. CONCLUSION

(Note: Contents of this chapter first appeared in [2].)

We have assessed IR+microwave retrievals from the existing AIRS/AMSU retrieval system and the v7 Stochastic Cloud Clearing/Neural Network (SCC/NN) [17, 18] first guess in comparison to collocated radiosondes. [2]

We first reviewed the current AIRS/AMSU retrieval methodology and how it utilizes a neural network and physical retrieval in combination. We then described the recently introduced consensus equilibrium framework, highlighting how it generalizes traditional Bayesian optimal estimation techniques to include new, powerful prior models. We showed how new moisture retrievals developed under MIT-LL's 2017 TASNPP effort can be viewed as special case of this framework, leading to significant improvements in PBL vertical detail, including sharp gradients at the top of the PB. This new methodology balances sensor physics with a prior model informed by machine learning[26]. We have also applied modern deep learning techniques to enhance convective PBL detail in a 3D volume of hyperspectral IR/microwave retrievals, also showing promising quantitative improvement in subkilometer PBLH estimation. [2]

While encouraged by this recent progress, we hypothesize that significant further improvement in retrieval of T and q in the PBL is possible by expanding on these approaches. The ESAS 2017 outlines numerous high priority scientific questions that will be addressed with improved observations of the PBL, and our ongoing work, by improving global retrieval accuracy and resolution from POR systems, will offer cross-cutting benefit across all of them. [2]

7. REFERENCES

1. Milstein, A.B., J.A. Santanello, and W.J. Blackwell, *Detail Enhancement of AIRS/AMSU Temperature and Moisture Profiles Using a 3D Deep Neural Network.* Artificial Intelligence for the Earth Systems, 2023. **2**(220037).
2. Milstein, A.B. *Planetary Boundary Layer (PBL)*. 2022; Available from: https://apps.dtic.mil/sti/citations/trecms/AD1166514.
3. National Academies of Sciences, E. and Medicine, *Thriving on Our Changing Planet: A Decadal Strategy for Earth Observation from Space*. 2018, Washington, DC: The National Academies Press. 716.
4. *Planetary Boundary Layer Decadal Survey Incubation Study Team*. Available from: https://science.nasa.gov/earth-science/decadal-pbl.
5. Teixeira, J., et al., *Toward a Global Planetary Boundary Layer Observing System: The NASA PBL Incubation Study Team Report*. 2021.
6. Liu, H. and J. Li, *An Improvement in Forecasting Rapid Intensification of Typhoon Sinlaku (2008) Using Clear-Sky Full Spatial Resolution Advanced IR Soundings.* Journal of Applied Meteorology and Climatology, 2010. **49**(4): p. 821-827.
7. Pangaud, T., et al., *Assimilation of AIRS Radiances Affected by Mid- to Low-Level Clouds.* Monthly Weather Review, 2009. **137**(12): p. 4276-4292.
8. Martins, J.P.A., et al., *Infrared sounding of the trade-wind boundary layer: AIRS and the RICO experiment.* Geophysical Research Letters, 2010. **37**(24).
9. Rodgers, C.D., *Inverse Methods for Atmospheric Sounding: Theory and Practice*. 2000: World Scientific Publishing Company, Incorporated.
10. Irion, F.W., et al., *Single-footprint retrievals of temperature, water vapor and cloud properties from AIRS.* Atmos. Meas. Tech., 2018. **11**(2): p. 971-995.
11. Blackwell, W.J. and F.W. Chen, *Neural Networks in Atmospheric Remote Sensing*. 2009: Artech House, Incorporated.
12. Hornik, K., *Approximation capabilities of multilayer feedforward networks.* Neural Networks, 1991. **4**(2): p. 251-257.
13. Maddy, E.S. and S.A. Boukabara, *MIIDAPS-AI: An Explainable Machine-Learning Algorithm for Infrared and Microwave Remote Sensing and Data Assimilation Preprocessing - Application to LEO and GEO Sensors.* IEEE Journal of Selected Topics in Applied Earth Observations and Remote Sensing, 2021. **14**: p. 8566-8576.
14. Cai, X., et al., *Temperature and Humidity Profile Retrieval from FY4-GIIRS Hyperspectral Data Using Artificial Neural Networks.* Remote Sensing, 2020. **12**(11): p. 1872.
15. Aires, F., et al., *Remote sensing from the infrared atmospheric sounding interferometer instrument 2. Simultaneous retrieval of temperature, water vapor, and ozone atmospheric profiles.* Journal of Geophysical Research: Atmospheres, 2002. **107**(D22): p. ACH 7-1-ACH 7-12.
16. Blackwell, W.J. and F.W. Chen, *Neural network applications in high-resolution atmospheric remote sensing.* Lincoln Laboratory Journal, 2005. **15**(2): p. 299-322.
17. Blackwell, W.J. and A.B. Milstein, *A Neural Network Retrieval Technique for High-Resolution Profiling of Cloudy Atmospheres.* 2014. **7**(4): p. 1260-70.
18. Milstein, A.B. and W.J. Blackwell, *Neural network temperature and moisture retrieval algorithm validation for AIRS/AMSU and CrIS/ATMS.* Journal of Geophysical Research: Atmospheres, 2016.
19. Susskind, J., J.M. Blaisdell, and L. Iredell, *Improved methodology for surface and atmospheric soundings, error estimates, and quality control procedures: the atmospheric infrared sounder science team version-6 retrieval algorithm.* J. Appl. Remote Sens., 2014. **8**: p. 084994 (33 pp.).

20. Ferguson, C.R., J.A. Santanello, and P. Gentine, *Enhanced Soundings for Local Coupling Studies Field Campaign Report*, R. Stafford, Editor. 2016: DOE ARM Climate Research Facility, DOE/SC-ARM-16-023.
21. Afonso, M.V., J.M. Bioucas-Dias, and M.A.T. Figueiredo, *Fast Image Recovery Using Variable Splitting and Constrained Optimization.* IEEE Transactions on Image Processing, 2010. **19**(9): p. 2345-2356.
22. Bouman, C.A., *Model-Based Image Processing*. 2017: https://engineering.purdue.edu/bouman/publications/pdf/MBIP-book.pdf.
23. Buzzard, G.T., et al., *Plug-and-Play Unplugged: Optimization-Free Reconstruction Using Consensus Equilibrium.* SIAM J. Imaging Sci., 2017. **11**(3): p. 2001-2020.
24. Strow, L.L., et al., *An overview of the AIRS radiative transfer model.* Geoscience and Remote Sensing, IEEE Transactions on, 2003. **41**(2): p. 303-313.
25. Liu, X., et al. *Retrieving atmospheric temperature and moisture profiles from SUOMI NPP CrIS/ATMS sensors using CrIMSS EDR algorithm*. in *Geoscience and Remote Sensing Symposium (IGARSS), 2012 IEEE International*. 2012.
26. Milstein, A.B., W.J. Blackwell, and J.A. Santanello. *Neural Network Techniques to Improve Infrared Sounding of the Atmosphere* in *19th Symposium on the Coastal Environment, 20th Conference on Artificial Intelligence for Environmental Science* 2021. AMS.
27. Tao, Z., W.J. Blackwell, and D.H. Staelin, *Error Variance Estimation for Individual Geophysical Parameter Retrievals.* 2013. **51**(3): p. 1718-27.
28. Karl, W.C., *3.6 - Regularization in Image Restoration and Reconstruction*, in *Handbook of Image and Video Processing (Second Edition)*, A.L. Bovik, Editor. 2005, Academic Press: Burlington. p. 183-V.
29. Ronneberger, O., P. Fischer, and T. Brox. *U-Net: Convolutional Networks for Biomedical Image Segmentation*. 2015; Available from: https://arxiv.org/abs/1505.04597.
30. Lu, Z. and Y. Chen. *Single Image Super Resolution based on a Modified U-net with Mixed Gradient Loss*. 2019; Available from: https://arxiv.org/abs/1911.09428.
31. Seidel, D.J., C.O. Ao, and K. Li, *Estimating climatological planetary boundary layer heights from radiosonde observations: Comparison of methods and uncertainty analysis*. Journal of Geophysical Research: Atmospheres, 2010. **115**(D16).
32. Guo, J., et al., *Investigation of near-global daytime boundary layer height using high-resolution radiosondes: first results and comparison with ERA5, MERRA-2, JRA-55, and NCEP-2 reanalyses.* Atmos. Chem. Phys., 2021. **21**(22): p. 17079-17097.